Visible Light Photoredox-Catalyzed Decarboxylative Alkylation of 3-Aryl-Oxetanes and Azetidines via Benzylic Tertiary Radicals and Implications of Benzylic Radical Stability

Maryne, A. J. Dubois,[a,†] Juan J. Rojas,[a,†] Alistair J. Sterling,[b,†] Hannah C. Broderick,[a] Milo, A. Smith,[a] Andrew J. P. White,[a] Philip W. Miller,[a] Chulho Choi,[c] James, J. Mousseau,[c] Fernanda Duarte,*[,b] and James, A. Bull*[,a]

[a] Department of Chemistry, Imperial College London, Molecular Sciences Research Hub, White City Campus, Wood Lane, London W12 0BZ, UK.

[b] Department of Chemistry, Chemistry Research Laboratory, University of Oxford, Oxford, UK.

[c] Pfizer Global Research and Development, 445 Eastern Point Rd., Groton, CT 06340, USA.

† These authors contributed equally.

Supporting Information Placeholder

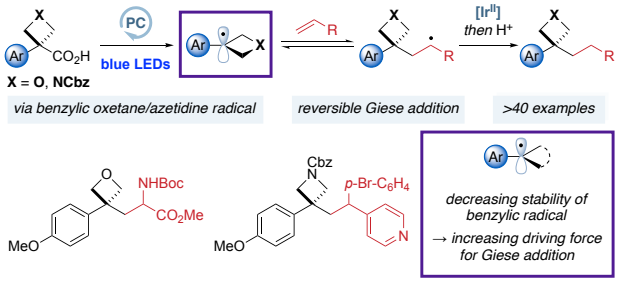

ABSTRACT: 4-Membered ring heterocycles oxetanes and azetidines offer exciting potential as small polar molecular motifs in medicinal chemistry but require further methods for their incorporation. Photoredox catalysis has emerged as a powerful method for the mild generation of alkyl radicals for C–C bond-forming reactions. However, the reactivity of radicals on strained rings is not well understood and there are few studies that address this question systematically. Furthermore, examples that use tertiary and benzylic radicals are rare, and their reactivity is challenging to harness and direct towards productive reaction pathways. This work develops a radical functionalization of benzylic oxetanes and azetidines using visible light photoredox catalysis to prepare 3-aryl-3-alkyl substituted derivatives and assesses the influence of ring strain on the reactivity of medicinally important small-ring radicals. 3-Aryl-3-carboxylic acid oxetanes and azetidines are suitable precursors for the formation of tertiary benzylic oxetane/azetidine radicals with loss of CO_2 and subsequent conjugate addition into activated alkenes. The process is shown to be tolerant of polar functional groups and heterocycles to generate medicinally relevant compounds bearing oxetane or azetidine motifs. We compare the reactivity of the oxetane radicals with that of other common benzylic systems. Computational studies indicate the Giese addition of benzylic radicals into acrylates to be generally reversible, resulting in lower yields and radical dimerization. However, the oxetane structure provides an overall exergonic process for the Giese addition step of the benzylic radical. Furthermore, strained ring structures benefit from lower spin density at the benzylic position, which is crucial to minimize radical dimerization. The lower spin density results from more extensive radical delocalization into the aromatic system which is rationalized on the basis of hybridization. The effect of radical acceptor on the distribution of products is investigated and a mechanism for the formation of side products of reduction is proposed based on experimental and computational evidence.

Oxetanes and azetidines continue to attract interest as valuable motifs in medicinal chemistry.[1] These motifs have increasingly appeared in clinical candidates, including Lanraplenib,[2] Crenolanib,[3] and FDA-approved Siponimod[4] and Baricitinib (Figure 1).[5] The low molecular weight and high polarity of 4-membered heterocycles can provide attractive molecular properties, as well as replacement groups for sensitive and metabolically exposed functionalities.[1,6] 3,3-Disubstituted oxetanes in particular present interesting opportunities as bioisosteres, providing comparable features to carbonyl groups and advantages due to increased steric protection, which improves stability to nucleophiles and acidic conditions. The attractive features of 4-membered rings have prompted the development of several new

approaches for their synthesis and late-stage incorporation to overcome the challenges posed by their ring strain and potential instability.[7]

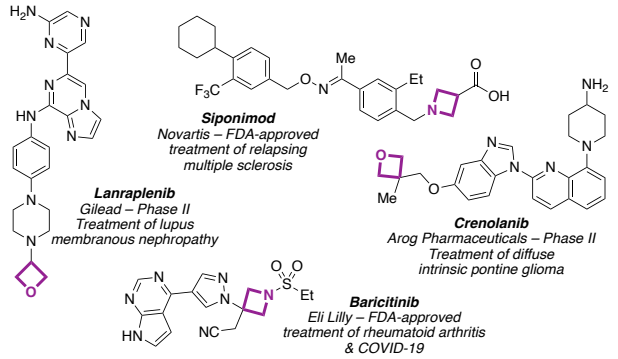

Figure 1. Oxetane and azetidine-containing pharmaceuticals.

Recent years have seen developments in the generation and reaction of oxetane and azetidine radicals as reactive intermediates. Radicals have been generated from oxetane itself and azetidine derivatives at the activated C2-position where the radical is stabilized by the adjacent lone pair.[8] Radical generation at the 3-position must compete with possible HAT processes at the more stable 2-position and hence requires a group that can act as radical precursor.[9-16] Recently, oxetane functionalization has been achieved using visible light mediated photoredox catalysis which has emerged as a powerful and general tool to generate radical species under mild conditions.[17] 3-Iodo-oxetane and azetidine are increasingly employed in coupling reactions,[9,10] while there are only limited examples from oxetane-3-carboxylic acid. To date there have been very few and isolated examples of tertiary oxetane radicals at the 3-position (Scheme 1).

In 2014, Ravelli reported the generation of 3-methyloxetane radicals by decarbonylation using UV light and TBADT ($[(n\text{-Bu})_4N]_4[W_{10}O_{32}]$), and their reaction with Michael acceptors.[8a] In 2018, Frenette and Pfizer developed visible light conditions for Minisci reactions.[11] Also in 2018, Shenvi used HAT/Ni dual catalysis to hydroarylate oxetane alkylidenes with aryl halides *via* a 3-alkyloxetane radical.[13] In 2020, Huestis reported the synthesis of 3-aryl-3-amino oxetanes and azetidines through the photocatalytic generation and coupling of 3-amino radical intermediates with aryl halides.[14] Very recently, 3-silyloxy azetidine and oxetane radicals were reported by Shen from 3-silyl azetidin-3-ols and oxetan-3-ols through a radical 1,2-silyl transfer which underwent C–C coupling with Michael acceptors.[15]

Following our interest in 3-aryloxetane and azetidine derivatives involving carbocation intermediates,[18] we envisaged that benzylic oxetane radicals would broaden the range of options for oxetane incorporation and provide access to valuable, unexplored and medicinally relevant chemical space under mild photoredox conditions. However, tertiary benzylic radicals remain underinvestigated in photoredox catalysis[19] and might be expected to display low reactivity in their addition reactions due to their relatively stabilized nature.[20] To date, there have been no reports of the reaction of 3-aryloxetane[21] or azetidine radicals, and the effect of the 4-membered ring on the reactivity and radical structure were unclear at the outset of this work.

Scheme 1. Strategies for the formation of 3,3-disubstituted oxetanes and azetidines by radical functionalization.

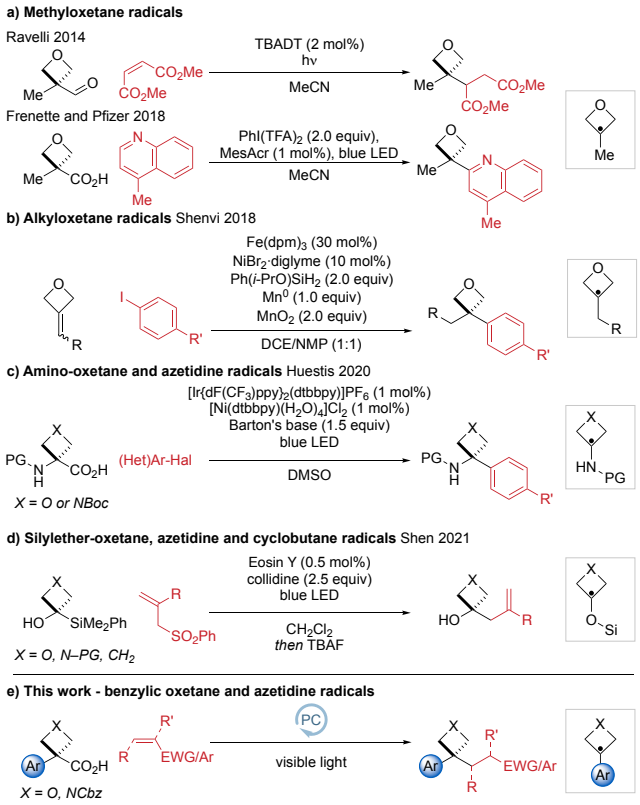

Here, we report our studies on the formation and reactions of oxetane and azetidine radicals using visible light mediated photoredox catalysis starting from carboxylic acid derivatives. We also report a systematic comparison of reaction outcomes for related substituted benzylic radicals and highlight important structural features for the reactivity of benzylic radicals. Most notably, we draw correlations between radical stability and the equilibrium of the reversible Giese addition, based on factors of hybridization.

We first investigated several possible radical precursors, initially derived from oxetanols. Attempts to prepare 3-aryloxetane derivatives of typical radical precursors such as bromide and chloride were unsuccessful (Supporting Scheme S3) and similarly, borate or silicate derivatives are not readily available. Oxalates, as the acid or Cs-salt[22] were prone to hydrolysis under reaction conditions and parallel screening of conditions did not provide a productive reaction (Supporting Scheme S4 and Table S1). We hence examined oxetane carboxylic acids. Carboxylic acids have been extensively used in the formation of tertiary radical centers under photocatalytic conditions.[23-25] Aryloxetane carboxylic acids were not available and prompted our recent report on their short two-step synthesis from 3-aryl-oxetan-3-ols involving catalytic Friedel–Crafts reaction followed by mild oxidative cleavage.[26,27] Initial investigations with acid **1** were based on a report by MacMillan in 2014[28] which generated C(sp^3) radicals under decarboxylative photoredox conditions and trapped these with electron deficient alkenes.[29] Electron-rich oxetane acid **1** was used as model substrate and ethyl acrylate as radical acceptor. Notably,

given the relative value of the oxetane acid derivative, we used the olefin in excess, which is uncommon in photoredox chemistry.[30] The major product of this reaction was 3,3-disubstituted oxetane **2a**, which was formed alongside di-alkylated product **2a'**, dimer **3** and reduced product **4**. After an extensive survey of discrete and continuous reaction variables (Supplementary Tables S2 and S3), desired 3,3-disubstituted oxetane **2a** was obtained in 61% yield (± 5%, 95% confidence interval, n = 6, performed by three different chemists; Table 1, entry 1), with minimized formation of side products (**3**, **4**).

Table 1. Selected optimization studies for the reaction of oxetane acid 1 with ethyl acrylate.

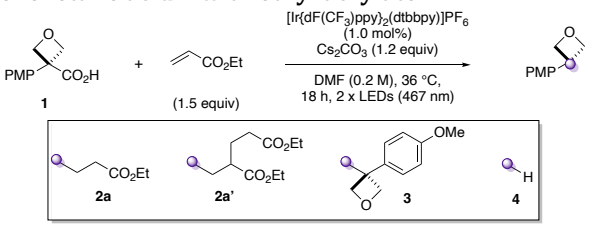

entry	change from standard conditions	yield (%)[a] 2a	2a'	3	4
1[b]	None	61 (58)	8 (8)	1	1
2	cat. = $Ru(bpy)_3(PF_6)_2$	<5	0	2	0
3	cat. = Mes-Acr$^+$	0	0	0	0
4	0.5 mol% Ir cat.	46	11	2	0
5[c]	28 °C (fan cooling)	54	11	3	0
6	solvent = MeCN	41	7	2	1
7	solvent = 1,4-dioxane	28	3	3	1
8	[0.1 M]	59	15	2	3
9	DBU as base	39	4	2	1
10	No photocatalyst	0	0	0	0
11	No light	0	0	0	0
12	No base	0	0	0	0

[a] Reactions run on a 0.2 mmol scale under argon. Yield calculated by analysis of the ^{1}H NMR spectrum of the crude mixture of the reaction using 1,3,5-trimethoxybenzene as internal standard and a 30 s relaxation delay (d1). [b] Reported yields are the mean average of 6 experiments, isolated yields of a single run are in parentheses. [c] Temperature recorded when the reaction was cooled with a fan. PMP = *p*-methoxyphenyl.

The optimized conditions used two readily available 467 nm LED Kessil lamps, Cs_2CO_3 as base and DMF as reaction solvent (see the Supporting Information page S6 for a detailed description of the reaction set-up). Iridium photocatalyst $[Ir\{dF(CF_3)ppy\}_2(dtbbpy)]PF_6$ (**[Ir]**; see Scheme 2) provided appropriate redox potentials to oxidize the carboxylate and reduce the Giese adduct. Other photocatalysts such as $[Ru(bpy)_3](PF_6)_2$ or (Mes-Acr)(ClO_4) formed little (<5%) or no product (entries 2–3). Only slight reductions in yield were observed when reducing photocatalyst loading to 0.5 mol% (entry 4), performing the reaction at lower temperatures (28 °C, fan controlled; entry 5), in different solvents (MeCN, 1,4-dioxane; entries 6–7), lower concentration (entry 8) or with an organic base (DBU; entry 9). Control experiments demonstrated the requirement for photocatalyst, light and base (entries 10–12). We examined deviations in reaction conditions that are often encountered between laboratories using a sensitivity screen as described by Glorius (Figure 2).[31] The reaction was shown to be broadly insensitive to small changes in the optimized conditions, thus facilitating implementation of the decarboxylative oxetane-functionalization protocol (see Supplementary Table S5 for details). Only high concentrations (0.25 instead of 0.2 M) and high levels of oxygen (i.e. under air) were identified as potential pitfalls for the reaction, factors that can be readily controlled. Notably, given the known sensitivity of photochemical reactions to increased scale,[32] the input of **1** could be increased to 5 times the standard scale (0.2 to 1.0 mmol) by simply increasing the size of the reaction vial with no impact on yield (58% of **2a**).

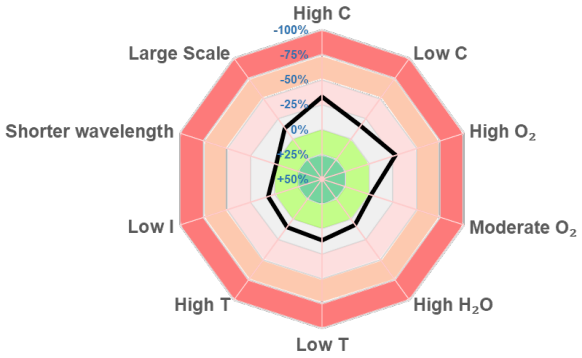

Figure 2. Assessment of sensitivity of the reaction of oxetane acid 1 with ethyl acrylate. Numbers indicate the deviation in percentage yield on alteration of selected reaction parameters.

With optimized and reliable conditions in hand, the scope of the reaction was probed (Scheme 2). A diverse set of novel 3,3-disubstituted oxetane products was swiftly obtained varying both the radical acceptor and the oxetane acid precursor. Simple acrylates were successful coupling partners and generated the products in good yields (**2a**, **2b**). A ketone was successfully incorporated in moderate yield (**2c**) and less electron-deficient alkenes such as vinyl sulfones, phosphonates and nitriles could also be employed, albeit in lower yields (**2d**–**2f**). Medicinally-interesting amide derivatives were synthesized in moderate to high yields (**2g**–**2i**). Similarly, a radical acceptor with two stabilizing groups was well tolerated using protected dehydroalanine to generate unnatural amino acid **2j**. Methacrolein was also successful, providing aldehyde **2k**. Substitution at the β-position was less well tolerated, though successful reactions were achieved with cyclopentenone and dimethyl maleate, affording **2l** and **2m** in 25% and 54% yield respectively. Styrenes were also successful coupling partners (**2n**–**2t**). Unactivated, electron-neutral styrene yielded oxetane **2n** in 32% yield. Reactivity increased with more electron-poor acceptors whereby *p*-bromophenyl (73%) and isobenzofuranone (60%) functionalities were incorporated efficiently (**2o**, **2p**). The tolerance of an aryl bromide group is noteworthy, especially since it serves as a synthetic handle for downstream diversifications. Importantly, pyridines, the most prevalent aromatic N-heterocycles in bioactive compounds,[33] could be readily introduced whilst tolerating functionalities such as a secondary amide (**2q**–**2t**).

Scheme 2. Reaction scope of oxetane and azetidine acids and alkenes[a]

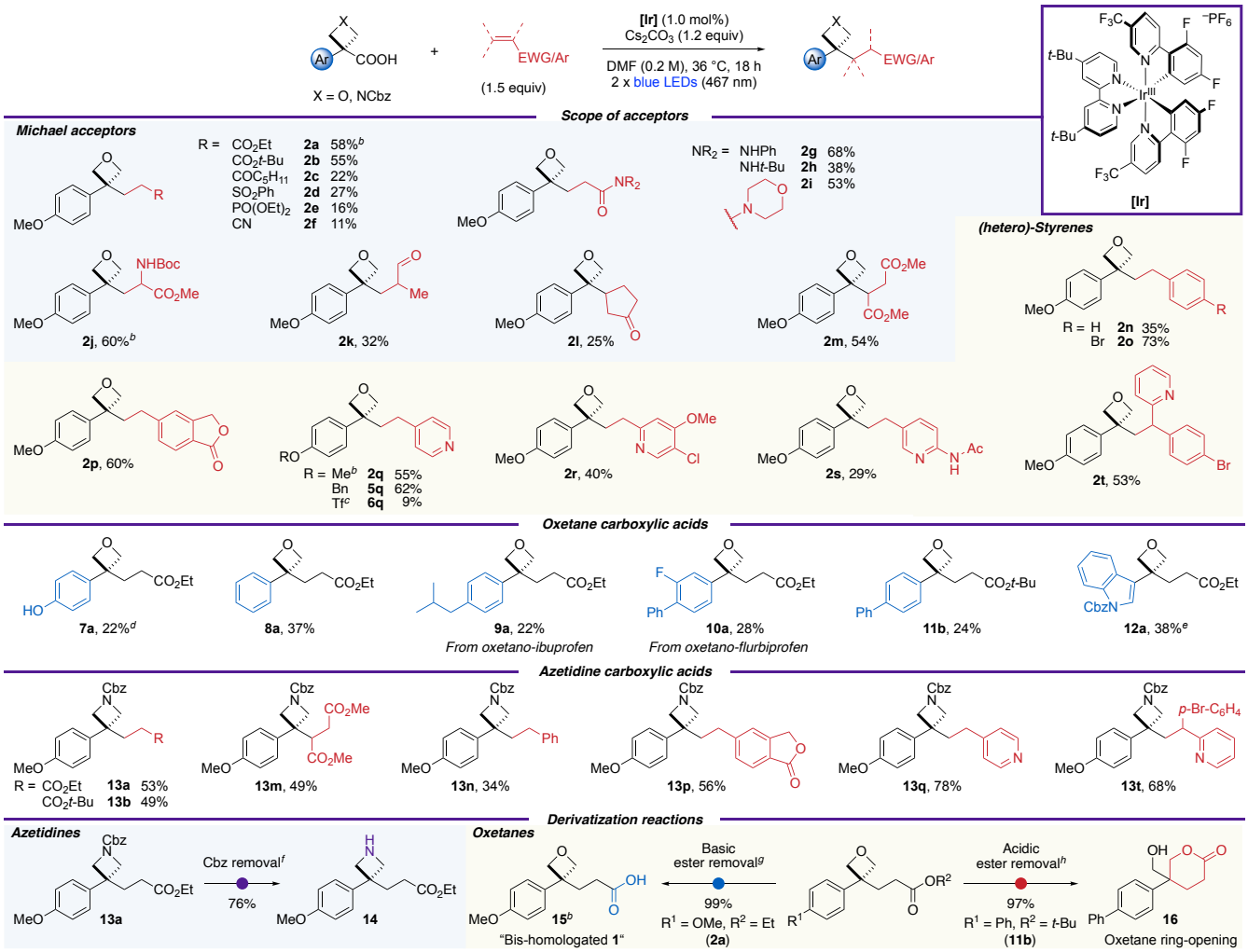

[a] Reactions run on a 0.20 mmol scale unless otherwise stated. Isolated yields are reported. [b] Characterized by X-ray crystallography. [c] Isolated in 70% purity. [d] Using TIPS-protected oxetane acid. [e] 0.1 mmol scale. [f] H_2, Pd/C (10% *w/w*, 10 mol% Pd), EtOH, 25 °C, 22 h. [g] LiOH (3.0 equiv), H_2O:THF:MeOH (3:1:1), 25 °C, 24 h. [h] Trifluoroacetic acid (10 equiv), CH_2Cl_2, 0–25 °C, 17 h.

Next, variation in the oxetane acids was investigated (**5**–**12**). A benzyl protecting group, which can be labile to photoredox conditions,[34] was well tolerated (**5q**; 62%). An electron-withdrawing triflate group could also be incorporated in low yields (**6q**; see Figure 5 for further discussion). TIPS-protected phenol was deprotected under the reaction conditions to give free phenol **7a**. Importantly, and in contrast to our previous strategies generating oxetane carbocations,[18] electron-neutral phenyl oxetane acid was a successful substrate and provided 3,3-disubstituted oxetane **8a** in 37% yield. Electron-neutral oxetane analogs of ibuprofen and flurbiprofen gave oxetanes **9a** and **10a**, and unsubstituted biphenyl oxetane acid gave an oxetane-containing ester analog of fenbufen (**11b**). The medicinally important indole group was also incorporated (**12a**).

Pleasingly, 3-arylazetidine radicals could also be formed under the reaction conditions and a range of 3,3-disubstituted azetidines were synthesized in comparable yields to their oxetane analogs (**13a**, **b**, **m**, **n**, **p**, **q**, **t**). Azetidine pyridines **13q** and **13t** showed a boost in yield compared to the oxetanes.

The Cbz group could be readily removed from **13a** by hydrogenolysis to generate a free N–H azetidine (**14**; 76% yield). Ester hydrolysis from the functionalized oxetane products under basic conditions using LiOH gave carboxylic acid **15** in 99% yield.[35] This is the formal bis-homologation product of oxetane **1**, which was further characterized by X-ray crystallography (see Supporting Figure S28). Interestingly, deprotection of the *t*-Bu ester **11b** using trifluoroacetic acid prompted ring-opening of the oxetane ring to form tetrahydropyranone **16** in 97% yield due to the internal nucleophile.

3,3-Disubstitued oxetanes **2a**, **2j** and **2q** were further characterized by X-ray crystallography and compared to known analogous phenone structures, which displayed interesting differences in conformation (Figure 3, also see Supplementary Information pages S69–S77). The 3,3-disubstituted oxetane derivatives adopt a conformation with increased 3-dimensional nature. Most notably the aromatic ring on the oxetane is almost orthogonal to the pseudo-carbonyl plane ($O_{oxetane}$-$Cq_{oxetane}$-$Cq_{aromatic}$), whilst in the ketone, the aromatic ring is aligned with the plane as to maximize favorable π-conjugation.

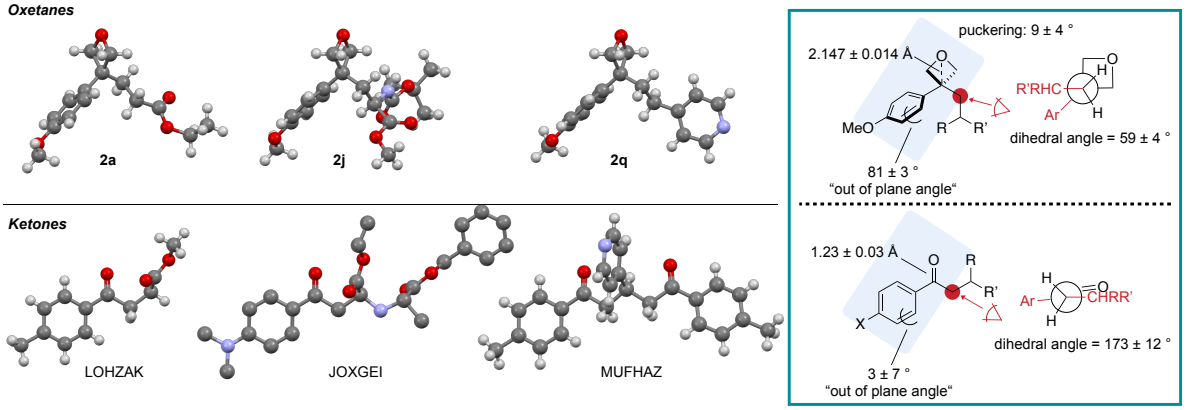

Figure 3. X-Ray structures of 3-aryl-3-alkyl oxetanes. Interatomic distances and torsion angles are given as the mean average of the three X-ray structures displayed with the error corresponding to the 95% confidence interval (for the oxetanes and ketones respectively). The ketone structures were accessed under the CCDC identifiers 'LOHZAK',[36] 'JOXGEI'[37] and 'MUFHAZ'.[38]

Furthermore, the increased steric bulk of the oxetane group together with the decreased steric requirement of the 'twisted' aromatic ring induce a switch in the preferred conformation of the CH_2CHRR' chain, which now lies on the side of the aromatic instead of the carbonyl (oxetane).

Based on the precedent of decarboxylative photoredox reactions[25a–d, 28] we propose an oxetane/azetidine radical intermediate formed by oxidation of the carboxylate anion with the excited form of the photocatalyst followed by decarboxylation (see Scheme S6 for the proposed mechanism). Reacting oxetane **1** with ethyl acrylate in the presence of TEMPO did not form the usual product **2a**. Oxetane–TEMPO adduct **17** was instead isolated in 21% yield (after chromatography) and its structure confirmed by X-ray crystallography, supporting the proposed oxetane radical (Scheme 3a). The radical is likely to undergo conjugate addition to the alkene, which is further reduced to a stabilized anion (*e.g.* an enolate when using ethyl acrylate) to turn over the Ir catalyst. Formation of the proposed enolate is supported by the reduction potential of the Giese adduct, which was calculated to lie well within the range of Ir^{II} (Scheme 3b).

A final protonation step would yield the observed products. A deuterium labelling study of the reaction of oxetane acid **1** with ethyl acrylate under the standard conditions showed deuterium incorporation alpha to the ethyl ester only with D_2O as additive, supporting the involvement of a protonation instead of an H-atom transfer step (Scheme 3c).[39] No deuterium incorporation was observed with DMF-d_7 or deuterated oxetane acid ***d*-1** (COOD). Quenching with D_2O at the end of the reaction showed no deuterium incorporation, suggestive of enolate protonation during the course of the reaction by water generated from the protonation of Cs_2CO_3.[40]

Scheme 3. Mechanistic studies[a]

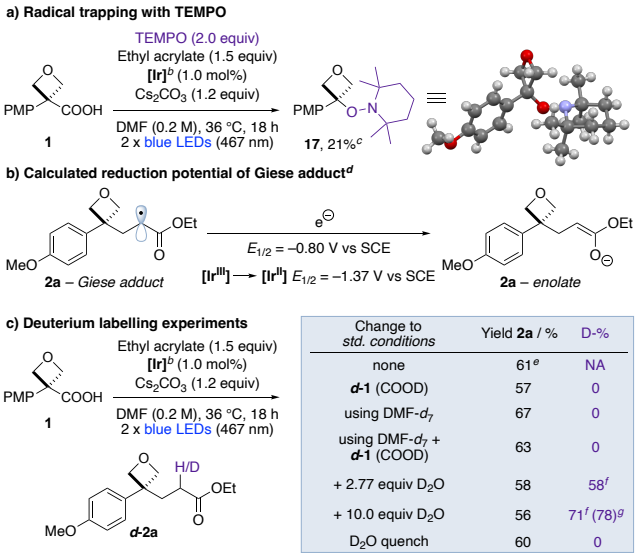

Change to *std. conditions*	Yield **2a** / %	D-%
none	61[e]	NA
***d*-1** (COOD)	57	0
using DMF-d_7	67	0
using DMF-d_7 + ***d*-1** (COOD)	63	0
+ 2.77 equiv D_2O	58	58[f]
+ 10.0 equiv D_2O	56	71[f] (78)[g]
D_2O quench	60	0

[a] Yield and percentage of deuteration (D-%) calculated by analysis of the ^1H NMR spectrum of the crude mixture of the reaction using 1,3,5-trimethoxybenzene as internal standard and a 30 s relaxation delay (d1). [b] **[Ir]** = [Ir{dF(CF$_3$)ppy}$_2$(dtbbpy)]PF$_6$ (see Scheme 2). [c] Isolated yield. [d] Value calculated using the methyl ester at the SMD(DMF)-M06-2X/ma-def2-TZVP//ωB97X-D3/def2-SVP level (298.15 K, 1 M). Reduction potential of Ir^{III} taken from ref 41. [f] Relevant signals in the ^1H NMR spectrum of the crude reaction mixture obscured by other species. Approximate value given. [g] Degree of deuteration measured after isolation by column chromatography. [e] Average of six experiments. NA = Not applicable.

Intermolecular reactions that involve radicals at benzylic positions often lead to low yields of the desired product and increased side reactions such as homo-coupling or reduction.[12,19c,20,42] The reasons behind this, and the effect of additional substituents at the benzylic position on reactivity, are not well understood. To provide insight into the key radical-addition step, we compared the behavior of a series of aryl acetic acids, with different substitution at the benzylic center, in the reaction with ethyl acrylate (Scheme 4). Only oxetane and azetidine undergo the desired Giese reaction

pathway efficiently (>50% **2a** = **III-A**, and **13a** = **IV-A**). Very little or no dimer formation was observed for the 3- and 4-membered rings, in contrast to methylene, *gem*-dimethyl and tetrahydropyran linkers.[43]

Scheme 4. Reactivity of tertiary benzylic radicals[a]

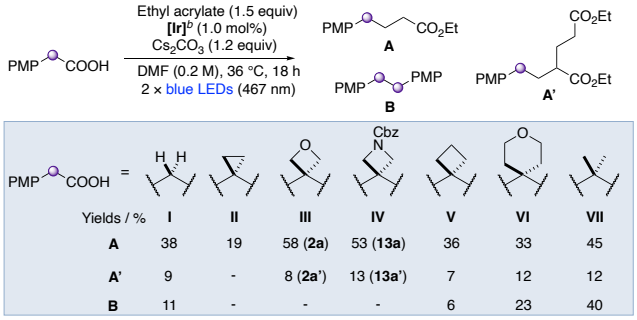

Yields / %	I	II	III	IV	V	VI	VII
A	38	19	58 (**2a**)	53 (**13a**)	36	33	45
A'	9	-	8 (**2a'**)	13 (**13a'**)	7	12	12
B	11	-	-	-	6	23	40

[a] Isolated yields are reported. [b] **[Ir]** = [Ir{dF(CF$_3$)ppy}$_2$(dtbbpy)]PF$_6$ (see Scheme 2).

These significant differences in reactivity of aryl acetic acids with different benzylic linkers was further investigated computationally to provide insights into the underlying features that lead to these disparities. Since maximizing the yield of Giese product requires minimization of undesired dimerization, we sought to identify the origins of dimer formation. The relative quantities of dimer observed vary significantly depending on the identity of the benzylic substituents (Scheme 4). We isolated two factors that minimize dimer formation: (1) decreasing the stability of the benzylic radical, and (2) enhancing π-delocalization of the benzylic radical into the aromatic system.

First, and perhaps surprisingly, computations showed the Giese addition of benzylic radicals into methyl acrylate to be reversible (Figure 4a). The relative stability of the benzylic radicals was then calculated (relative to cyclopropane radical **II**; Figure 4b) and found to directly influence the quantity of dimer through the equilibrium position of the Giese addition, with a linear relationship (R^2 = 0.87, Figure 4c). As the radical becomes less stable, the driving force for the Giese addition increases and dimerization is disfavored (Figure 4d). For example, the relative instability of cyclopropyl radical **II** causes an exergonic addition to the acrylate (ΔG = –11.7 kcal mol^{-1}), resulting in rapid Giese quenching of this radical and therefore dimer suppression. The cyclopropane radical however, is known to be very unstable and more prone to ring opening than its larger-ring counterparts, presumably leading to its increased degradation and consequently, a low yield of Giese product **II-A** (19%).[44] Conversely, the *gem*-dimethyl benzylic radical **VII** is stabilized to the extent that the addition to the acrylate becomes endergonic (ΔG = +0.6 kcal mol^{-1}), allowing a build-up of this radical in the reaction and increasing the likelihood of dimerization (Figure 4e).

The unsubstituted benzylic radical (**I**) is an outlier in this stability/dimerization trend in that dimer is observed (11%), despite the equilibrium lying towards the Giese adduct (ΔG = –4.4 kcal mol^{-1}). To explain this phenomenon, we noted that the spin density is much more localized at the benzylic position than that of the rest of the radicals under study (ρ_s = 0.75, Figure 4f). More localized benzylic radicals incur a lower penalty to dimerization, making unsubstituted radical **I** the most susceptible to dimerization of the series.[45,46] On the other hand, the lower spin density of the cyclopropane radical **II** (ρ_s = 0.67) increases the barrier to dimerization relative to the Giese addition.

We propose that the extent of radical delocalization is controlled by the hybridization of the arene-to-benzylic-carbon σ bond (Figure 4g), which in turn is determined by the hybridization of the C–C σ bonds of the additional benzylic substituents (Figure 4h). Substrates in which these benzylic C–C bonds *require* enhanced p-character due to the small internal angles of small rings, *e.g.* cyclopropane **II** (sp$^{3.75}$; Figure 4h), must assign greater s-character to the arene-to-benzylic-carbon C–C σ bond (sp$^{1.25}$; Figure 4g). This is expressed in a shorter C–C bond, increased radical delocalization and reduced benzylic spin density (Figure 4i; see Figure 4j for our proposed model for variation in spin density). We propose that delocalization is enhanced in oxetane **III** compared to cyclobutane **V** due to Bent's rule[47]: the electronegative oxetane oxygen atom withdraws electron density from the ring C–C bonds, forcing a greater p-contribution to these bonds in **III** than **V** (sp$^{3.40}$ vs sp$^{3.15}$, respectively, Figure 4h). As a result, the arene-to-benzylic-carbon C–C bond in **III** is richer in s-character (sp$^{1.37}$) and shorter (1.404 Å) than in **V** (sp$^{1.53}$ and 1.410 Å, respectively), thereby increasing π-delocalization and subsequently minimizing dimerization.

Overall, dimerization will be minimized for substrates with destabilized benzylic radicals that are able to efficiently delocalize into the arene π system. For example, the Giese addition for oxetane radical **III** is exergonic (ΔG = –3.7 kcal mol^{-1}), and the radical is sufficiently π-delocalized (ρ_s = 0.67) due to the high p-character demanded within the oxetane ring (*vide supra*), such that no dimer is observed and the yield of Giese product is high in the reaction with acrylates.

Computationally, the substituents on the arene were found to have little influence on the stability, spin density and Giese equilibrium of the benzylic radical (Figure 5a). This is in accordance with the experimental distribution of products, where exclusively Giese product was observed for electronically different oxetane carboxylic acids (*i.e.* neither dimerization nor reduction products observed). The yield however, varied significantly, with a positive correlation between aromatic electron-density and yield (yield **2a**>**8a**>>**6q**; Scheme 2). Ravelli showed relatively electron-poor benzylic carboxylates to be harder to oxidize than more electron-rich examples.[20a] We measured the oxidation potential of three electronically different 3-aryl-oxetane carboxylates by cyclic voltammetry and found the same trend (Figure 5b).[48] It is feasible that the less favorable carboxylate oxidation is responsible for the lower yield observed with acid substrates bearing less electron-rich aryl rings.[49] The subsequent decarboxylation step, which has been shown to be "ultrafast" (k = 10^{10} s^{-1}),[50] is unlikely to play a significant role. Less electron-rich oxetane radicals are also less nucleophilic, which may correlate to the CV data, and could result in a slower Giese addition step. More oxidizing photocatalysts were tested with the Ph-oxetane carboxylate but there was no increase in yield of **8a** (0% with [Ru(bpz)$_3$](PF$_6$)$_2$ {+1.45 V}[17a] and 31% with 4CzIPN {+1.35 V}[42b]; Supporting Table S3).

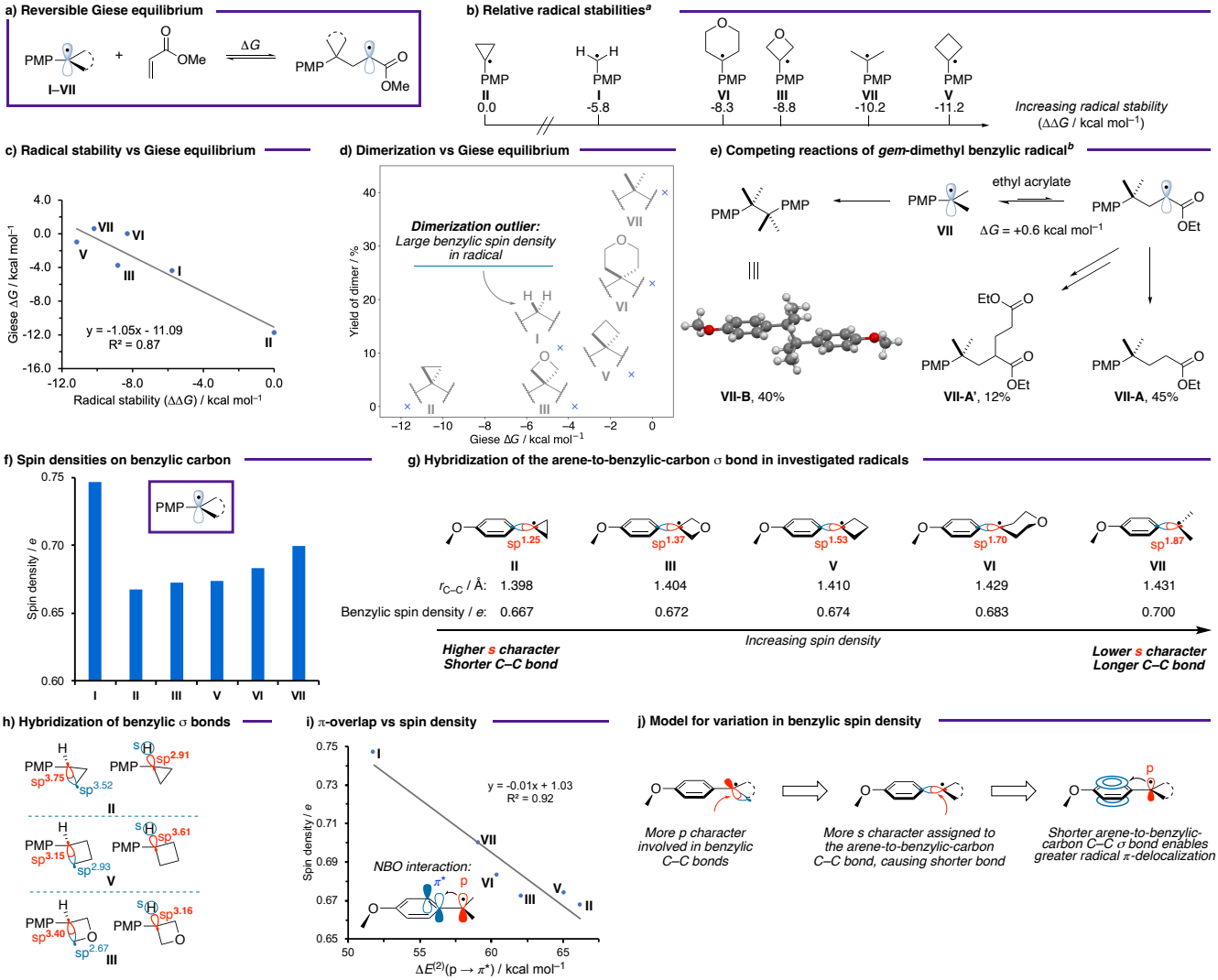

Figure 4. Analysis of the reactivity of benzylic radicals in a Giese-type reaction. All calculations at the CPCM(DMF)-ωB97X-D3/def2-TZVP//ωB97X-D3/def2-SVP level. Free energies calculated at 298.15 K and 1 M standard state. [a] Stabilities determined through H-atom exchange equilibria with cyclopropyl radical **II** (Supporting Figure S20). [b] ΔG calculated using methyl acrylate (Supporting Figure S21).

a) Calculated properties of 3-aryl-oxetane radicals[a]

	R = OMe	R = H	R = CF_3
Stability (ΔΔG / kcal mol⁻¹)	–8.8	–8.2	–8.9
Benzylic spin density (e)	0.672	0.679	0.668
Giese equilibrium (ΔG / kcal mol⁻¹)	–3.7	–3.7	–2.6

b) Measured oxidation potentials of oxetane carboxylates[b]

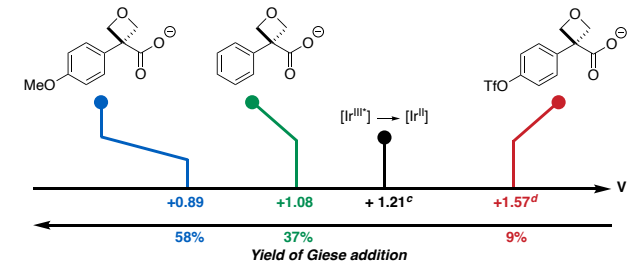

Figure 5. Effect of aryl group on the Giese-type reaction. [a] All calculations at the CPCM(DMF)-ωB97X-D3/def2-TZVP//ωB97X-D3/def2-SVP level (298.15 K, 1 M, Supporting Table S9). Stabilities relative to PMP-cyclopropyl radical **II**. Giese equilibrium with methyl acrylate as radical acceptor. *p*-CF_3-phenyl chosen as model electron-poor aromatic. [b] Oxidation potentials measured by cyclic voltammetry in a 0.1 M solution of NBu_4ClO_4 in MeCN at 25 °C with 100 mV s^{-1} scan rate and reported vs SCE. Carboxylates generated *in situ* through the addition of 1 equiv NBu_4OH (1 M in MeOH). Here, the anodic peak potentials (E_{pa}) are reported.[51] See the Supporting Information, page S22 for further details. [c] Value refers to $\mathbf{E_{1/2}^{III*/II}}$, taken from ref 41. [d] Estimated value, see Supporting Table S8 and Figure S11. Further oxidations at low potentials were observed for this compound.

Investigation of the reaction scope showed a stark influence of the radical acceptor on the distribution of products (**P**:**3**:**4**; Scheme 5a). Particularly, less electrophilic and/or more sterically hindered alkenes led to increased amounts oxetane dimer **3** and reduced oxetane **4**. This is presumably, and in line with our calculations (see discussion above and Figure 4), due to the reversible Giese addition where less activated alkenes shift the equilibrium towards the oxetane

radical. This shift results in a higher concentration of oxetane radical which significantly increases the rate of dimerization, which is directly proportional to the square of radical concentration, and the formation of reduced oxetane **4**. In the absence of a radical acceptor only minimal amounts of side products **3** and **4** were observed (Scheme 5a), hinting to involvement of the acceptor in the catalytic cycle and in regeneration of the Ir^{III} catalyst, as is calculated to occur with the Giese adduct of **2a** to regenerate Ir^{III} (Scheme 3b). However, direct oxidation of Ir^{II} ($E_{1/2}^{Ir^{III}/Ir^{II}}$ = –1.37 V vs SCE)[41] by the alkene is unfeasible based on calculated reduction potentials (*e.g.* for cyclohexene methyl carboxylate: $E_{1/2}^{M/M^{\bullet-}}$ = –2.60 V vs SCE; see Supporting Table S9 for all calculated values).[52] Thus, more likely, the high concentration of strained oxetane radical also increases the rate of irreversible oxetane degradation pathways to generate radicals that can more easily add into the acceptor and form unidentified Giese adducts capable of oxidizing Ir^{II}.[53]

Finally, we considered the mechanism to form reduced oxetane **4**, which occurs in the absence of an explicit reductant or H-atom transfer (HAT) reagent. Deuteration studies suggest H_2O, generated from the protonation of Cs_2CO_3, to be the primary source of hydrogen incorporated into the 3-position of **4** (Scheme 5b). The low deuterium incorporation with DMF-d_7 rules out HAT from DMF to the oxetane radical.[54] Direct HAT from water is also unlikely due to the high bond dissociation energy of the H–OH bond (>115 kcal mol^{-1}).[55] Reduction of the oxetane radical by Ir^{II} to an *unstable* oxetane-3-anion followed by protonation is unfeasible based on the expected instability of the anionic intermediate and the calculated reduction potential of the oxetane radical ($E_{1/2}^{III/III^{-}}$ = –1.67 V vs SCE) which lies outside the reduction range of Ir^{II} (Scheme 5b). Based on the above computational and experimental observations, we propose reduced oxetane **4** to be generated through a concerted multisite proton-coupled electron transfer (PCET)[56] with water as source of protons and Ir^{II} as source of electrons (Scheme 5b, see Scheme S6 for the full mechanistic picture).

Scheme 5. Influence of radical acceptor on preferred reaction pathway[a]

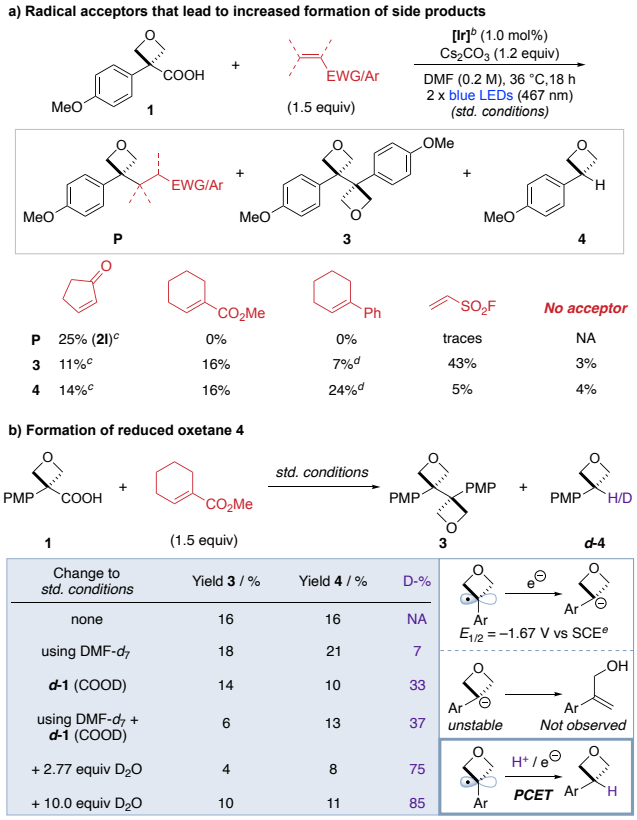

[a] Yield and percentage of deuteration (D-%) calculated by analysis of the ^{1}H NMR spectrum of the crude mixture of the reaction using 1,3,5-trimethoxybenzene as internal standard and a 30 s relaxation delay (d1). [b] **[Ir]** = [Ir{dF(CF_3)ppy}$_2$(dtbbpy)]PF_6 (see Scheme 2). [c] Isolated yields. [d] Estimated yields based on the mass of the crude reaction mixture and the ratio of **3** and **4** in the ^{1}H NMR spectrum. [e] Value calculated at the SMD(DMF)-M06-2X/madef2-TZVP//ωB97X-D3/def2-SVP level (298.15 K, 1 M). NA = Not applicable.

In summary, we report the generation of unusual tertiary benzylic strained oxetane and azetidine radicals under photoredox catalysis. We have developed a protocol for the use of 3-aryl-3-carboxylic acid oxetanes and azetidines as radical precursors which react with alkenes to form medicinally-relevant alkylated 3,3-disubstituted oxetanes and azetidines with previously inaccessible substitution patterns. The reaction is reproducible, easy to set up and insensitive to common deviations from the conditions. The products could be further transformed to reveal free NH azetidine functionality, as well as a free "bis-homologated" oxetane carboxylic acid or a tetrahydropyranone heterocycle after oxetane ring-opening, depending on the conditions used for ester removal. An experimental comparison of the reactivity of different benzylic radicals revealed only oxetane and azetidine substrates to favor a productive Giese reaction pathway with the other benzylic linkers showing significantly lower yields and/or increased amounts of dimer side products. A computational investigation revealed the Giese addition of benzylic radicals into acrylate

acceptors to be reversible, with less stable radicals shifting the equilibrium towards the coupled product. Furthermore, reduced spin density on the benzylic carbon was found to minimize formation of the dimer side product. Oxetane and azetidine radicals are the only species that lie in the sweet spot of little degradation of the benzylic radical, whilst showing an exergonic Giese addition and minimal dimer formation. Studies are presented to explain the differing reaction outcome with certain acceptors, and to suggest the origin of side products of reduction. We envisage this protocol will encourage the use of 3-aryl-3-carboxylic acid oxetanes and azetidines as convenient radical precursors in medicinal chemistry and expand the medicinal chemist's toolbox for the incorporation of 4-membered rings into drug-like compounds.

ASSOCIATED CONTENT

Supporting Information

X-ray crystallographic data; detailed optimization and sensitivity tables; further discussion of mechanism and scope; cyclic voltammetry (CV) measurements; experimental procedures, detailed description of set-up, characterization data and copies of ^{1}H, ^{13}C, ^{19}F and ^{31}P NMR spectra (PDF)

Accession Codes

CCDC 2184087–2184092 contain the supplementary crystallographic data for this paper. These data can be obtained free of charge via www.ccdc.cam.ac.uk/data_request/cif, or by emailing data_request@ccdc.cam.ac.uk, or by contacting The Cambridge Crystallographic Data Centre, 12 Union Road, Cambridge CB2 1EZ, UK; fax: +44 1223 336033.

AUTHOR INFORMATION

Corresponding Authors

* E-mail: j.bull@imperial.ac.uk
* E-mail: fernanda.duartegonzalez@chem.ox.ac.uk

Notes

The authors declare no competing financial interest.

ACKNOWLEDGMENT

We gratefully acknowledge The Royal Society [University Research Fellowship, UF140161 and URF\R\201019 (to J.A.B.), URF Appointed Grant RG150444 and URF Enhancement Grant RGF\EA\180031], Pfizer and Imperial College London for studentship funding (M.D. and J.J.R.) and EPSRC Centre for Doctoral training in Next Generation Synthesis and Reaction Technology (EP/S023232/1) for a studentship to H.A.B]. We thank Richard P. Loach and Thomas Knauber (Pfizer) for valuable discussion and training. A. J. S. thanks the EPSRC Centre for Doctoral Training in Synthesis for Biology and Medicine for a studentship (EP/L015838/1), the Oxford-Radcliffe Scholarship for a studentship, and the EPSRC Doctoral Prize (EP/T517811/1) for support. This work used the Cirrus UK National Tier-2 HPC Service at EPCC (http://www.cirrus.ac.uk) funded by the University of Edinburgh and EPSRC (EP/P020267/1).

REFERENCES

(1) (a) Burkhard, J. A.; Wuitschik, G.; Rogers-Evans, M.; Müller, K.; Carreira, E. M. Oxetanes as Versatile Elements in Drug Discovery and Synthesis. *Angew. Chem. Int. Ed.* **2010**, *49*, 9052–9067. (b) Carreira, E. M.; Fessard, T. C. Four-Membered Ring-Containing Spirocycles: Synthetic Strategies and Opportunities. *Chem. Rev.* **2014**, *114*, 8257–8322. (c) Bull, J. A.; Croft, R. A.; Davis, O. A.; Doran, R.; Morgan, K. F. Oxetanes: Recent Advances in Synthesis, Reactivity, and Medicinal Chemistry. *Chem. Rev.* **2016**, *116*, 12150–12233. (d) Kirichok, A. A.; Shton, I.; Kliachyna, M.; Pishel, I.; Mykhailiuk, P. K. 1-Substituted 2-Azaspiro[3.3]Heptanes: Overlooked Motifs for Drug Discovery. *Angew. Chem. Int. Ed.* **2017**, *56*, 8865–8869. (e) Bott, T. M.; West, F. G. Preparation and Synthetic Applications of Azetidines. *Heterocycles* **2012**, *84*, 223–264. (f) Rojas, J. J.; Bull, J. A. Oxetanes and Oxetenes-Monocyclic. In *Comprehensive Heterocyclic Chemistry IV*; Black, D. S.; Cossy, J.; Stevens, C. V., Eds.; Elsevier, 2022; Vol. *1*, pp 212–256.

(2) ClinicalTrials.gov Identifier: NCT03285711.

(3) ClinicalTrials.gov Identifier: NCT01229644.

(4) Chen, Z.; Doyle, T. M.; Luongo, L.; Largent-Milnes, T. M.; Giancotti, L. A.; Kolar, G.; Squillace, S.; Boccella, S.; Walker, J. K.; Pendleton, A.; Spiegel, S.; Neumann, W. L.; Vanderah, T. W.; Salvemini, D. Sphingosine-1-Phosphate Receptor 1 Activation in Astrocytes Contributes to Neuropathic Pain. *Proc. Natl. Acad. Sci.* **2019**, *116*, 10557–10562.

(5) (a) FDA-approval against rheumatoid arthritis: Application Number: 207924. First global approval: Markham, A. Baricitinib: First Global Approval. *Drugs* **2017**, *77*, 697–704. (b) As treatment against COVID-19: Stebbing, J.; Sánchez Nievas, G.; Falcone, M.; Youhanna, S.; Richardson, P.; Ottaviani, S.; Shen, J. X.; Sommerauer, C.; Tiseo, G.; Ghiadoni, L.; Virdis, A.; Monzani, F.; Romero Rizos, L.; Forfori, F.; Avendaño Céspedes, A.; De Marco, S.; Carrozzi, L.; Lena, F.; Sánchez-Jurado, P. M.; Lacerenza, L. G.; Cesira, N.; Caldevilla Bernardo, D.; Perrella, A.; Niccoli, L.; Sáez Méndez, L.; Matarrese, D.; Goletti, D.; Tan, Y.-J.; Monteil, V.; Dranitsaris, G.; Cantini, F.; Farcomeni, A.; Dutta, S.; Burley, S. K.; Zhang, H.; Pistello, M.; Li, W.; Mas Romero, M.; Andrés Pretel, F.; Sánchez Simón-Talero, R.; García-Molina, R.; Kutter, C.; Felce, J. H.; Nizami, Z. F.; Miklosi, A. G.; Penninger, J. M.; Menichetti, F.; Mirazimi, A.; Abizanda, P.; Lauschke, V. M. JAK Inhibition Reduces SARS-CoV-2 Liver Infectivity and Modulates Inflammatory Responses to Reduce Morbidity and Mortality. *Sci. Adv.* **2021**, *7*, eabe4724.

(6) (a) Wuitschik, G.; Carreira, E. M.; Wagner, B.; Fischer, H.; Parrilla, I.; Schuler, F.; Rogers-Evans, M.; Müller, K. Oxetanes in Drug Discovery: Structural and Synthetic Insights. *J. Med. Chem.* **2010**, *53*, 3227–3246. (b) Dubois, M. A. J.; Croft, R. A.; Ding, Y.; Choi, C.; Owen, D. R.; Bull, J. A.; Mousseau, J. J. Investigating 3,3-Diaryloxetanes as Potential Bioisosteres through Matched Molecular Pair Analysis. *RSC Med. Chem.* **2021**. 12, 2045–2052.

(7) For selected examples, see: (a) Becker, M. R.; Wearing, E. R.; Schindler, C. S. Synthesis of Azetidines via Visible-Light-Mediated Intermolecular [2+2] Photocycloadditions. *Nat. Chem.* **2020**, *12*, 898–905. (b) Rykaczewski, K. A.; Schindler, C. S. Visible-Light-Enabled Paternò–Büchi Reaction via Triplet Energy Transfer for the Synthesis of Oxetanes. *Org. Lett.* **2020**, *22*, 6516–6519. (c) Davis, O. A.; Bull, J. A. Synthesis of Di-, Tri-, and Tetrasubstituted Oxetanes by Rhodium-Catalyzed O–H Insertion and C–C Bond-Forming Cyclization. *Angew. Chem. Int. Ed.* **2014**, *53*, 14230–14234. (d) Willand-Charnley, R.; Puffer, B. W.; Dussault, P. H. Oxacycle Synthesis via Intramolecular Reaction of Carbanions and Peroxides. *J. Am. Chem. Soc.* **2014**, *136*, 5821–5823. (e) Davis, O. A.; Croft, R. A.; Bull, J. A. Synthesis of Diversely Functionalised 2,2-Disubstituted Oxetanes: Fragment Motifs in New Chemical Space. *Chem. Commun.* **2015**, *51*, 15446–15449. (f) Butova, E. D.; Barabash, A. V.; Petrova, A. A.; Kleiner, C. M.; Schreiner, P. R.; Fokin, A. A. Stereospecific Consecutive Epoxide Ring Expansion with Dimethylsulfoxonium Methylide. *J. Org. Chem.* **2010**, *75*, 6229–6235. (g) Rodina, L. L.; Malashikhin, S. A.; Galkina, O. S.; Nikolaev, V. A. Photochemical Reactions of Regioisomeric 2,2-Dimethyl-5,5-Diphenyl- and 5,5-Dimethyl-2,2-Diphenyl-Substituted Diazo Ketones of a Tetrahydrofuran Series. *Helv. Chim. Acta* **2009**, *92*, 1990–1998. (h) Kovács, E.; Faigl, F.; Mucsi, Z. Regio- and Diastereoselective Synthesis of 2-Arylazetidines: Quantum Chemical Explanation of Baldwin's Rules for the Ring-Formation Reactions of Oxiranes. *J. Org. Chem.* **2020**, *85*,

11226–11239. (i) Gianatassio, R.; Lopchuk, J. M.; Wang, J.; Pan, C.-M.; Malins, L. R.; Prieto, L.; Brandt, T. A.; Collins, M. R.; Gallego, G. M.; Sach, N. W.; Spangler, J. E.; Zhu, H.; Zhu, J.; Baran, P. S. Strain-Release Amination. *Science* **2016**, *351*, 241–246. Also see reference 18.

(8) (a) Ravelli, D.; Zoccolillo, M.; Mella, M.; Fagnoni, M. Photocatalytic Synthesis of Oxetane Derivatives by Selective C–H Activation. *Adv. Synth. Catal.* **2014**, *356*, 2781–2786. (b) Jin, J.; MacMillan, D. W. C. Direct α-Arylation of Ethers through the Combination of Photoredox-Mediated C–H Functionalization and the Minisci Reaction. *Angew. Chem. Int. Ed.* **2015**, *54*, 1565–1569.

(9) For selected examples, using iodooxetane in Minisci reactions, see: (a) Duncton, M. A. J.; Estiarte, M. A.; Johnson, R. J.; Cox, M.; O'Mahony, D. J. R.; Edwards, W. T.; Kelly, M. G. Preparation of Heteroaryloxetanes and Heteroarylazetidines by Use of a Minisci Reaction. *J. Org. Chem.* **2009**, *74*, 6354–6357. (b) Nuhant, P.; Oderinde, M. S.; Genovino, J.; Juneau, A.; Gagné, Y.; Allais, C.; Chinigo, G. M.; Choi, C.; Sach, N. W.; Bernier, L.; Fobian, Y. M.; Bundesmann, M. W.; Khunte, B.; Frenette, M.; Fadeyi, O. O. Visible-Light-Initiated Manganese Catalysis for C–H Alkylation of Heteroarenes: Applications and Mechanistic Studies. *Angew. Chem. Int. Ed.* **2017**, *56*, 15309–15313.

(10) (a) Górski, B.; Barthelemy, A.; Douglas, J. J.; Juliá, F.; Leonori, D. Copper-Catalysed Amination of Alkyl Iodides Enabled by Halogen-Atom Transfer. *Nat. Catal.* **2021**, *4*, 623–630. (b) Constantin, T.; Zanini, M.; Regni, A.; Sheikh, N. S.; Juliá, F.; Leonori, D. Aminoalkyl Radicals as Halogen-Atom Transfer Agents for Activation of Alkyl and Aryl Halides. *Science* **2020**, *367*, 1021–1026. (c) Kvasovs, N.; Iziumchenko, V.; Palchykov, V.; Gevorgyan, V. Visible Light-Induced Pd-Catalyzed Alkyl-Heck Reaction of Oximes. *ACS Catal.* **2021**, *11*, 3749–3754. (d) Bissonnette, N. B.; Boyd, M. J.; May, G. D.; Giroux, S.; Nuhant, P. C–H Functionalization of Heteroarenes Using Unactivated Alkyl Halides through Visible-Light Photoredox Catalysis under Basic Conditions. *J. Org. Chem.* **2018**, *83*, 10933–10940. (e) Ye, S.; Zheng, D.; Wu, J.; Qiu, G. Photoredox-Catalyzed Sulfonylation of Alkyl Iodides, Sulfur Dioxide, and Electron-Deficient Alkenes. *Chem. Commun.* **2019**, *55*, 2214–2217.

(11) Genovino, J.; Lian, Y.; Zhang, Y.; Hope, T. O.; Juneau, A.; Gagné, Y.; Ingle, G.; Frenette, M. Metal-Free-Visible Light C–H Alkylation of Heteroaromatics via Hypervalent Iodine-Promoted Decarboxylation. *Org. Lett.* **2018**, *20*, 3229–3232.

(12) 3-Methyloxetane radicals have also been generated by deoxygenation of an NHC-activated alcohol and coupled to aryl halides: Dong, Z.; MacMillan, D. W. C. Metallaphotoredox-Enabled Deoxygenative Arylation of Alcohols. *Nature* **2021**, *598*, 451–456.

(13) Green, S. A.; Vásquez-Céspedes, S.; Shenvi, R. A. Iron–Nickel Dual-Catalysis: A New Engine for Olefin Functionalization and the Formation of Quaternary Centers. *J. Am. Chem. Soc.* **2018**, *140*, 11317–11324.

(14) Kolahdouzan, K.; Khalaf, R.; Grandner, J. M.; Chen, Y.; Terrett, J. A.; Huestis, M. P. Dual Photoredox/Nickel-Catalyzed Conversion of Aryl Halides to Aryl Aminooxetanes: Computational Evidence for a Substrate-Dependent Switch in Mechanism. *ACS Catal.* **2020**, *10*, 405–411.

(15) Zhang, Y.; Zhang, Y.; Shen, X. Alkoxyl-Radical-Mediated Synthesis of Functionalized Allyl Tert-(Hetero)Cyclobutanols and Their Ring-Opening and Ring-Expansion Functionalizations. *Chem Catal.* **2021**, *1*, 423–436.

(16) Murray, P. R. D.; Bussink, W. M. M.; Davies, G. H. M.; van der Mei, F. W.; Antropow, A. H.; Edwards, J. T.; D'Agostino, L. A.; Ellis, J. M.; Hamann, L. G.; Romanov-Michailidis, F.; Knowles, R. R. Intermolecular Crossed [2 + 2] Cycloaddition Promoted by Visible-Light Triplet Photosensitization: Expedient Access to Polysubstituted 2-Oxaspiro[3.3]Heptanes. *J. Am. Chem. Soc.* **2021**, *143*, 4055–4063.

(17) For selected reviews on photoredox catalysis, see: (a) Prier, C. K.; Rankic, D. A.; MacMillan, D. W. C. Visible Light Photoredox Catalysis with Transition Metal Complexes: Applications in Organic Synthesis. *Chem. Rev.* **2013**, *113*, 5322–5363. (b) Roslin, S.; Odell, L. R. Visible-Light Photocatalysis as an Enabling Tool for the Functionalization of Unactivated C(sp^3)-Substrates. *Eur. J. Org. Chem.* **2017**, *2017*, 1993–2007. (c) Marzo, L.; Pagire, S. K.; Reiser, O.; König, B. Visible-Light Photocatalysis: Does It Make a Difference in Organic Synthesis? *Angew. Chem. Int. Ed.* **2018**, *57*, 10034–10072. (d) McAtee, R. C.; McClain, E. J.; Stephenson, C. R. J. Illuminating Photoredox Catalysis. *Trends Chem.* **2019**, *1*, 111–125. (e) Petzold, D.; Giedyk, M.; Chatterjee, A.; König, B. A Retrosynthetic Approach for Photocatalysis. *Eur. J. Org. Chem.* **2020**, *2020*, 1193–1244. (f) Cannalire, R.; Pelliccia, S.; Sancineto, L.; Novellino, E.; Tron, G. C.; Giustiniano, M. Visible Light Photocatalysis in the Late-Stage Functionalization of Pharmaceutically Relevant Compounds. *Chem. Soc. Rev.* **2021**, *50*, 766–897. (g) Li, P.; Terrett, J. A.; Zbieg, J. R. Visible-Light Photocatalysis as an Enabling Technology for Drug Discovery: A Paradigm Shift for Chemical Reactivity. *ACS Med. Chem. Lett.* **2020**, *11*, 2120–2130.

(18) (a) Croft, R. A.; Mousseau, J. J.; Choi, C.; Bull, J. A. Structurally Divergent Lithium Catalyzed Friedel–Crafts Reactions on Oxetan-3-ols: Synthesis of 3,3-Diaryloxetanes and 2,3-Dihydrobenzofurans. *Chem. Eur. J.* **2016**, *22*, 16271–16276. (b) Croft, R. A.; Mousseau, J. J.; Choi, C.; Bull, J. A. Lithium-Catalyzed Thiol Alkylation with Tertiary and Secondary Alcohols: Synthesis of 3-Sulfanyl-Oxetanes as Bioisosteres. *Chem. Eur. J.* **2018**, *24*, 818–821. (c) Denis, C.; Dubois, M. A. J.; Voisin-Chiret, A. S.; Bureau, R.; Choi, C.; Mousseau, J. J.; Bull, J. A. Synthesis of 3,3-Diarylazetidines by Calcium(II)-Catalyzed Friedel–Crafts Reaction of Azetidinols with Unexpected Cbz Enhanced Reactivity. *Org. Lett.* **2019**, *21*, 300–304. (d) Dubois, M. A. J.; Lazaridou, A.; Choi, C.; Mousseau, J. J.; Bull, J. A. Synthesis of 3-Aryl-3-Sulfanyl Azetidines by Iron-Catalyzed Thiol Alkylation with N-Cbz Azetidinols. *J. Org. Chem.* **2019**, *84*, 5943–5956. (e) Croft, R. A.; Dubois, M. A. J.; Boddy, A. J.; Denis, C.; Lazaridou, A.; Voisin-Chiret, A. S.; Bureau, R.; Choi, C.; Mousseau, J. J.; Bull, J. A. Catalytic Friedel-Crafts Reactions on Saturated Heterocycles and Small Rings for sp^3-sp^2 Coupling of Medicinally Relevant Fragments. *Eur. J. Org. Chem.* **2019**, *2019*, 5385–5395. (f) Rojas, J. J.; Croft, R. A.; Sterling, A. J.; Briggs, E. L.; Antermite, D.; Schmitt, D. C.; Blagojevic, L.; Haycock, P.; White, A. J. P.; Duarte, F.; Choi, C.; Mousseau, J. J.; Bull, J. A. Amino-Oxetanes as Amide Isosteres by an Alternative Defluorosulfonylative Coupling of Sulfonyl Fluorides. *Nat. Chem.* **2022**, *14*, 160–169. (g) Rojas, J. J.; Torrisi, E.; Dubois, M. A. J.; Hossain, R.; White, A. J. P.; Zappia, G.; Mousseau, J. J.; Choi, C.; Bull, J. A. Oxetan-3-ols as 1,2-Bis-Electrophiles in a Brønsted-Acid-Catalyzed Synthesis of 1,4-Dioxanes. *Org. Lett.* **2022**, *24*, 2365–2370.

(19) For isolated examples of tertiary benzylic radicals, see: a) Li, Z.; Wang, X.; Xia, S.; Jin, J. Ligand-Accelerated Iron Photocatalysis Enabling Decarboxylative Alkylation of Heteroarenes. *Org. Lett.* **2019**, *21*, 4259–4265. (b) Dang, H. T.; Haug, G. C.; Nguyen, V. T.; Vuong, N. T. H.; Nguyen, V. D.; Arman, H. D.; Larionov, O. V. Acridine Photocatalysis: Insights into the Mechanism and Development of a Dual-Catalytic Direct Decarboxylative Conjugate Addition. *ACS Catal.* **2020**, *10*, 11448–11457. (c) Shatskiy, A.; Axelsson, A.; Stepanova, E. V.; Liu, J.-Q.; Temerdashev, A. Z.; Kore, B. P.; Blomkvist, B.; Gardner, J. M.; Dinér, P.; Kärkäs, M. D. Stereoselective Synthesis of Unnatural α-Amino Acid Derivatives through Photoredox Catalysis. *Chem. Sci.* **2021**, *12*, 5430–5437. (d) Nguyen, V. T.; Haug, G. C.; Nguyen, V. D.; Vuong, N. T. H.; Arman, H. D.; Larionov, O. V. Photocatalytic Decarboxylative Amidosulfonation Enables Direct Transformation of Carboxylic Acids to Sulfonamides. *Chem. Sci.* **2021**, *12*, 6429–6436. (e) Feng, G.; Wang, X.; Jin, J. Decarboxylative C-C and C-N Bond Formation by Ligand-Accelerated Iron Photocatalysis. *Eur. J. Org. Chem.* **2019**, *2019*, 6728–6732. (f) Zhu, Q.; Nocera, D. G. Photocatalytic Hydromethylation and Hydroalkylation of Olefins Enabled by Titanium Dioxide Mediated Decarboxylation. *J. Am. Chem. Soc.* **2020**, *142*, 17913–17918. (g) Kautzky, J. A.; Wang, T.; Evans, R. W.; MacMillan, D. W. C. Decarboxylative Trifluoromethylation of Aliphatic Carboxylic Acids. *J. Am. Chem. Soc.* **2018**, *140*, 6522–6526. (h) Cao, H.; Jiang, H.; Feng, H.; Kwan, J. M. C.; Liu, X.; Wu, J. Photo-Induced Decarboxylative Heck-Type Coupling of Unactivated Aliphatic Acids and Terminal Alkenes in the Absence of

Sacrificial Hydrogen Acceptors. *J. Am. Chem. Soc.* **2018**, *140*, 16360–16367. (i) Nakagawa, M.; Nagao, K.; Ikeda, Z.; Reynolds, M.; Ibáñez, I.; Wang, J.; Tokunaga, N.; Sasaki, Y.; Ohmiya, H. Organophotoredox-Catalyzed Decarboxylative N-Alkylation of Sulfonamides. *ChemCatChem* **2021**, *13*, 3930–3933. (j) Kolusu, S. R. N.; Nappi, M. Metal-Free Deoxygenative Coupling of Alcohol-Derived Benzoates and Pyridines for Small Molecules and DNA-Encoded Libraries Synthesis. *Chem. Sci.* **2022**, *13*, 6982–6989.

(20) The increased stability of benzylic radicals, further increased for tertiary benzylic examples, often leads to homo-coupling reactions. The increased steric crowding around the reactive center also makes intermolecular reaction pathways less favorable for tertiary benzylic radials. (a) Capaldo, L.; Buzzetti, L.; Merli, D.; Fagnoni, M.; Ravelli, D. Smooth Photocatalyzed Benzylation of Electrophilic Olefins via Decarboxylation of Arylacetic Acids. *J. Org. Chem.* **2016**, *81*, 7102–7109. (b) Manley, D. W.; Walton, J. C. A Clean and Selective Radical Homocoupling Employing Carboxylic Acids with Titania Photoredox Catalysis. *Org. Lett.* **2014**, *16*, 5394–5397. (c) McLean, E. B.; Mooney, D. T.; Burns, D. J.; Lee, A.-L. Direct Hydrodecarboxylation of Aliphatic Carboxylic Acids: Metal- and Light-Free. *Org. Lett.* **2022**, *24*, 686–691.

(21) For a postulated intermediate 3-aryloxetane radical that was further oxidized to the carbocation, see: Li, P.; Zbieg, J. R.; Terrett, J. A. *ACS Catal.* **2021**, *11*, 10997–11004.

(22) (a) Nawrat, C. C.; Jamison, C. R.; Slutskyy, Y.; MacMillan, D. W. C.; Overman, L. E. Oxalates as Activating Groups for Alcohols in Visible Light Photoredox Catalysis: Formation of Quaternary Centers by Redox-Neutral Fragment Coupling. *J. Am. Chem. Soc.* **2015**, *137*, 11270–11273. (b) Zhang, X.; MacMillan, D. W. C. Alcohols as Latent Coupling Fragments for Metallaphotoredox Catalysis: sp^3–sp^2 Cross-Coupling of Oxalates with Aryl Halides. *J. Am. Chem. Soc.* **2016**, *138*, 13862–13865.

(23) For examples of the general use of carboxylic acids as radical precursors, see: (a) Roslin, S.; Odell, L. R. Visible-Light Photocatalysis as an Enabling Tool for the Functionalization of Unactivated C(sp^3)-Substrates. *Eur. J. Org. Chem.* **2017**, *2017*, 1993–2007. (b) Zuo, Z.; MacMillan, D. W. C. Decarboxylative Arylation of α-Amino Acids via Photoredox Catalysis: A One-Step Conversion of Biomass to Drug Pharmacophore. *J. Am. Chem. Soc.* **2014**, *136*, 5257–5260. (c) Noble, A.; McCarver, S. J.; MacMillan, D. W. C. Merging Photoredox and Nickel Catalysis: Decarboxylative Cross-Coupling of Carboxylic Acids with Vinyl Halides. *J. Am. Chem. Soc.* **2015**, *137*, 624–627. (d) Zuo, Z.; Ahneman, D. T.; Chu, L.; Terrett, J. A.; Doyle, A. G.; MacMillan, D. W. C. Merging Photoredox with Nickel Catalysis: Coupling of α-Carboxyl sp^3-Carbons with Aryl Halides. *Science* **2014**, *345*, 437–440. (e) Karmakar, S.; Silamkoti, A.; Meanwell, N. A.; Mathur, A.; Gupta, A. K. Utilization of C(sp^3)-Carboxylic Acids and Their Redox-Active Esters in Decarboxylative Carbon–Carbon Bond Formation. *Adv. Synth. Catal.* **2021**, *363*, 3693–3736.

(24) For seminal examples on the use of carboxylic acid derivatives as radical precursors for radical conjugate additions, see: (a) Barton, D. H. R.; Crich, D.; Kretzschmar, G. Formation of Carbon-Carbon Bonds with Radicals Derived from the Esters of Thiohydroxamic Acids. *Tetrahedron Lett.* **1984**, *25*, 1055–1058. (b) Barton, D. H. R.; Crich, D.; Kretzschmar, G. The Invention of New Radical Chain Reactions. Part 9. Further Radical Chemistry of Thiohydroxamic Esters; Formation of Carbon–Carbon Bonds. *J. Chem. Soc., Perkin Trans. 1* **1986**, 39–53.

(25) For examples on the use of carboxylic acids as radical precursors for radical conjugate additions using photocatalysis, see: (a) Yoshimi, Y.; Masuda, M.; Mizunashi, T.; Nishikawa, K.; Maeda, K.; Koshida, N.; Itou, T.; Morita, T.; Hatanaka, M. Inter- and Intramolecular Addition Reactions of Electron-Deficient Alkenes with Alkyl Radicals, Generated by SET-Photochemical Decarboxylation of Carboxylic Acids, Serve as a Mild and Efficient Method for the Preparation of γ-Amino Acids and Macrocyclic Lactones. *Org. Lett.* **2009**, *11*, 4652–4655. (b) Miyake, Y.; Nakajima, K.; Nishibayashi, Y. Visible Light-Mediated Oxidative Decarboxylation of Arylacetic Acids into Benzyl Radicals: Addition to Electron-Deficient Alkenes by Using Photoredox Catalysts. *Chem. Commun.* **2013**, *49*, 7854–7856. (c) Merkens, K.; Aguilar Troyano, F. J.; Djossou, J.; Gómez-Suárez, A. Synthesis of Unnatural α-Amino Acid Derivatives via Light-Mediated Radical Decarboxylative Processes. *Adv. Synth. Catal.* **2020**, *362*, 2354–2359. (d) Fernandez-Rodriguez, P.; Legros, F.; Maier, T.; Weber, A.; Méndez, M.; Derdau, V.; Hessler, G.; Kurz, M.; Villar-Garea, A.; Ruf, S. Photoinduced Decarboxylative Radical Addition Reactions for Late Stage Functionalization of Peptide Substrates. *Eur. J. Org. Chem.* **2021**, *2021*, 782–787. (e) Zhang, O.; Schubert, J. W. Derivatization of Amino Acids and Peptides via Photoredox-Mediated Conjugate Addition. *J. Org. Chem.* **2020**, *85*, 6225–6232.

(26) Dubois, M. A. J.; Smith, M. A.; White, A. J. P.; Lee Wei Jie, A.; Mousseau, J. J.; Choi, C.; Bull, J. A. Short Synthesis of Oxetane and Azetidine 3-Aryl-3-Carboxylic Acid Derivatives by Selective Furan Oxidative Cleavage. *Org. Lett.* **2020**, *22*, 5279–5283.

(27) For other methods to synthesize aryloxetane carboxylic acids, see: (a) Buckman, B. O.; Nicholas, J. B.; Emayan, K.; Seiwert, S. D. *Lysophosphatidic Acid Receptor Antagonists*. PCT Int. Appl. WO 2013025733 A1, February 21, 2013. (b) Li, D.; Sloman, D. L.; Achab, A.; Zhou, H.; McGowan, M. A.; White, C.; Gibeau, C.; Zhang, H.; Pu, Q.; Bharathan, I.; Hopkins, B.; Liu, K.; Ferguson, H.; Fradera, X.; Lesburg, C. A.; Martinot, T. A.; Qi, J.; Song, Z. J.; Yin, J.; Zhang, H.; Song, L.; Wan, B.; DAddio, S.; Solban, N.; Miller, J. R.; Zamlynny, B.; Bass, A.; Freeland, E.; Ykoruk, B.; Hilliard, C.; Ferraro, J.; Zhai, J.; Knemeyer, I.; Otte, K. M.; Vincent, S.; Sciammetta, N.; Pasternak, A.; Bennett, D. J.; Han, Y. Oxetane Promise Delivered: Discovery of Long-Acting IDO1 Inhibitors Suitable for Q3W Oral or Parenteral Dosing. *J. Med. Chem.* **2022**, *65*, 6001–6016.

(28) Chu, L.; Ohta, C.; Zuo, Z.; MacMillan, D. W. C. Carboxylic Acids as A Traceless Activation Group for Conjugate Additions: A Three-Step Synthesis of (±)-Pregabalin. *J. Am. Chem. Soc.* **2014**, *136*, 10886–10889.

(29) For reviews on Giese reactions and decarboxylative alkylations, see: (a) Gant Kanegusuku, A. L.; Roizen, J. L. Recent Advances in Photoredox-Mediated Radical Conjugate Addition Reactions: An Expanding Toolkit for the Giese Reaction. *Angew. Chem. Int. Ed.* **2021**, *60*, 21116–21149. (b) Kitcatt, D. M.; Nicolle, S.; Lee, A.-L. Direct Decarboxylative Giese Reactions. *Chem. Soc. Rev.* **2022**, 1415–1453. (c) Li, Y.; Ge, L.; Muhammad, M.; Bao, H. Recent Progress on Radical Decarboxylative Alkylation for Csp^3–C Bond Formation. *Synthesis* **2017**, *49*, 5263–5284.

(30) For example see reference 25c where the carboxylic acid had to be used in 10-fold excess for tertiary benzylic substrates (including cyclopropane and cyclobutane examples).

(31) Pitzer, L.; Schäfers, F.; Glorius, F. Rapid Assessment of the Reaction-Condition-Based Sensitivity of Chemical Transformations. *Angew. Chem. Int. Ed.* **2019**, *58*, 8572–8576.

(32) Bonfield, H. E.; Knauber, T.; Lévesque, F.; Moschetta, E. G.; Susanne, F.; Edwards, L. J. Photons as a 21st Century Reagent. *Nat. Commun.* **2020**, *11*, 804.

(33) Vitaku, E.; Smith, D. T.; Njardarson, J. T. Analysis of the Structural Diversity, Substitution Patterns, and Frequency of Nitrogen Heterocycles among U.S. FDA Approved Pharmaceuticals. *J. Med. Chem.* **2014**, *57*, 10257–10274.

(34) Cavedon, C.; Sletten, E. T.; Madani, A.; Niemeyer, O.; Seeberger, P. H.; Pieber, B. Visible-Light-Mediated Oxidative Debenzylation Enables the Use of Benzyl Ethers as Temporary Protecting Groups. *Org. Lett.* **2021**, *23*, 514–518.

(35) **1** was found to be stable under standard laboratory conditions (handling at room temperature, removal of solvent at 40 °C, acidic aq. conditions {pH 1 with dilute HCl}, growing of crystals by slow evaporation of $CDCl_3$ over several days) and required no special considerations. Aryl substituents in the 3-position of oxetane carboxylic acids have been shown to stabilize against ring opening of more labile oxetane-3-acetic acid derivatives. See: Chalyk, B.; Grynyova, A.; Filimonova, K.; Rudenko, T. V; Dibchak, D.; Mykhailiuk, P. K. Unexpected Isomerization of Oxetane-Carboxylic Acids. *Org. Lett.* **2022**, *24*, 4722–4728.

(36) Ali, S.; Qadeer, G.; Rama, N. H.; Wong, W.-Y. CCDC 712490: Experimental Crystal Structure Determination. **2008**, DOI: 10.5517/ccrxdkl.
(37) Arcadi, A.; Marinelli, F.; Adovasio, V.; Nardelli, M. CCDC 1189583: Experimental Crystal Structure Determination. **1993**.
(38) Senge, M. O., Gibbons, D.; Emandi, G. CCDC 1992782: Experimental Crystal Structure Determination. **2020**, DOI: 10.5517/ccdc.csd.cc24wn90.
(39) Water-promoted protonation has been previously postulated for the Giese reaction of arylacetic acids (ref. 20a).
(40) Remarkably, the yield of **2a** stayed unaffected by the addition of 10 equiv of water. Increasing the concentration of source of protons even further (DMF:H_2O 2:1 as solvent) did not lead to an increase in yield of **2a** (Supporting Table S2).
(41) Lowry, M. S.; Goldsmith, J. I.; Slinker, J. D.; Rohl, R.; Pascal, R. A.; Malliaras, G. G.; Bernhard, S. Single-Layer Electroluminescent Devices and Photoinduced Hydrogen Production from an Ionic Iridium(III) Complex. *Chem. Mater.* **2005**, *17*, 5712–5719.
(42) For examples of benzylic substrates showing decreased or alternative reactivity in radical reactions, see: (a) Suga, T.; Shimazu, S.; Ukaji, Y. Low-Valent Titanium-Mediated Radical Conjugate Addition Using Benzyl Alcohols as Benzyl Radical Sources. *Org. Lett.* **2018**, *20*, 5389–5392. (b) Ryder, A. S. H.; Cunningham, W. B.; Ballantyne, G.; Mules, T.; Kinsella, A. G.; Turner-Dore, J.; Alder, C. M.; Edwards, L. J.; McKay, B. S. J.; Grayson, M. N.; Cresswell, A. J. Photocatalytic α-Tertiary Amine Synthesis via C–H Alkylation of Unmasked Primary Amines. *Angew. Chem. Int. Ed.* **2020**, *59*, 14986–14991. (c) Ma, G.; Chen, C.; Talukdar, S.; Zhao, X.; Lei, C.-H.; Gong, H. Metal Catalyst-Free Photo-Induced Alkyl C–O Bond Borylation. *Chem. Commun.* **2020**, *56*, 10219–10222. (d) Askey, H. E.; Grayson, J. D.; Tibbetts, J. D.; Turner-Dore, J. C.; Holmes, J. M.; Kociok-Kohn, G.; Wrigley, G. L.; Cresswell, A. J. Photocatalytic Hydroaminoalkylation of Styrenes with Unprotected Primary Alkylamines. *J. Am. Chem. Soc.* **2021**, *143*, 15936–15945. (e) Suga, T.; Takahashi, Y.; Miki, C.; Ukaji, Y. direct and Unified Access to Carbon Radicals from Aliphatic Alcohols by Cost-Efficient Titanium-Mediated Homolytic C–OH Bond Cleavage. *Angew. Chem. Int. Ed.* **2022**, *61*, e202112533.
(43) The amount of di-addition product **A'**, formed through the addition of the product radical and/or enolate (**A**• or **A**$^-$) into another equivalent of ethyl acrylate (Supporting Scheme S6), was broadly similar across linkers that gave significant product formation (**I**, **III–VII**).
(44) Walsh, R. Cyclic Alkyl Radical Isomerization: A Correction to the Literature. *Int. J. Chem. Kinet.* **1970**, *2*, 71–74.
(45) Costentin, C.; Savéant, J. M. Origin of Activation Barriers in the Dimerization of Neutral Radicals: A "Nonperfect Synchronization" Effect? *J. Phys. Chem. A* **2005**, *109*, 4125–4132.
(46) Primary benzylic radicals have been shown to have a propensity to dimerize (ref. 20b).
(47) Bent, H. A. An Appraisal of Valence-Bond Structures and Hybridization in Compounds of the First-Row Elements. *Chem. Rev.* **1961**, *61*, 275–311.
Here, the electron-withdrawing effect of the electronegative oxygen atom on oxetane propagates through the two σ-bonds and imposes more s-character to the hybrid orbital responsible for the arene-to-benzylic-carbon σ bond. This shortens this bond and increases π delocalization of the benzylic radical. Bent's rule implies that the increased s-character in this bond is due to the unsymmetrical assignment of s and p character to hybrid orbitals to enable the electrons of polarized bonds to occupy lower energy orbitals, hence overall stabilization. This effect can be observed in the hybridization values in Figure 4h and is shown schematically below:

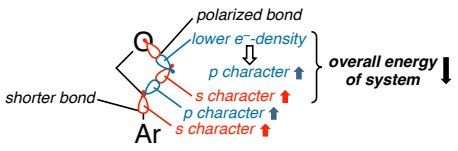

(48) The presence of the oxetane raised the oxidation potential of the PMP carboxylate (E_{pa} = +0.89 V) by +0.17/+0.16 V in comparison to the PMP carboxylates of cyclobutane (E_{pa} = +0.72 V) and *gem*-dimethyl (E_{pa} = +0.73 V) examples. The same trend was observed for phenyl carboxylates (E_{pa} oxetane/cyclobutane/*gem*-dimethyl = +1.08/+0.88/+0.92 V). See the Supporting Information, pages S23–S25 for further details.
(49) We note that *p*-OTf-phenyl oxetane carboxylate (see Figure 5b, Supporting Table S8 and Supporting Figure S11) showed several oxidation peaks at low potentials, suggestive of an oxidative degradation pathway for this substrate.
(50) Abel, B.; Assmann, J.; Buback, M.; Grimm, C.; Kling, M.; Schmatz, S.; Schroeder, J.; Witte, T. Ultrafast Decarboxylation of Carbonyloxy Radicals: Influence of Molecular Structure. *J. Phys. Chem. A* **2003**, *107*, 9499–9510.
(51) E_{pa} values provide more reliable and reproducible means to report the potentials of chemically irreversible oxidations (instead of *e.g.* estimating $E_{p/2}$ values), as suggested by Lam: Leech, M. C.; Lam, K. A Practical Guide to Electrosynthesis. *Nat. Rev. Chem.* **2022**, *6*, 275–286.
(52) A measured cyclic voltammogram of cyclohexene methyl carboxylate showed an oxidation at 2.12 V vs SCE but no significant reduction waves up to –3.0 V. See Supporting Figure S19 and Supporting Table S8.
(53) It has been recently shown that nucleophilic, C-centered, ring-opened oxetane radicals can efficiently react with electron-deficient alkenes in a Giese-type addition: Potrząsaj, A.; Ociepa, M.; Chaładaj, W.; Gryko, D. Bioinspired Cobalt-Catalysis Enables Generation of Nucleophilic Radicals from Oxetanes. *Org. Lett.* **2022**, *24*, 2469–2473.
(54) DMF has been previously shown to act as a hydrogen atom donor: (a) Salamone, M.; Milan, M.; DiLabio, G. A.; Bietti, M. Reactions of the Cumyloxyl and Benzyloxyl Radicals with Tertiary Amides. Hydrogen Abstraction Selectivity and the Role of Specific Substrate-Radical Hydrogen Bonding. *J. Org. Chem.* **2013**, *78*, 5909–5917. (b) Tam, C. M.; To, C. T.; Chan, K. S. Carbon–Carbon σ-Bond Transfer Hydrogenation with DMF Catalyzed by Cobalt Porphyrins. *Organometallics* **2016**, *35*, 2174–2177. (c) Samai, S.; Rouichi, S.; Ferhati, A.; Chakir, A. N,N-Dimethylformamide (DMF), and N,N-Dimethylacetamide (DMA) Reactions with NO_3, OH and Cl: A Theoretical Study of the Kinetics and Mechanisms. *Arab. J. Chem.* **2019**, *12*, 4957–4970.
(55) Ruscic, B.; Wagner, A. F.; Harding, L. B.; Asher, R. L.; Feller, D.; Dixon, D. A.; Peterson, K. A.; Song, Y.; Qian, X.; Ng, C.-Y.; Liu, J.; Chen, W.; Schwenke, D. W. On the Enthalpy of Formation of Hydroxyl Radical and Gas-Phase Bond Dissociation Energies of Water and Hydroxyl. *J. Phys. Chem. A* **2002**, *106*, 2727–2747.
(56) PCET is known to enable 'out-of-range' electron transfer processes. For reviews of PCET and its use in synthetic chemistry, see: a) Huynh, M. H. V; Meyer, T. J. Proton-Coupled Electron Transfer. *Chem. Rev.* **2007**, *107*, 5004–5064. b) Weinberg, D. R.; Gagliardi, C. J.; Hull, J. F.; Murphy, C. F.; Kent, C. A.; Westlake, B. C.; Paul, A.; Ess, D. H.; McCafferty, D. G.; Meyer, T. J. Proton-Coupled Electron Transfer. *Chem. Rev.* **2012**, *112*, 4016–4093. c) Miller, D. C.; Tarantino, K. T.; Knowles, R. R. Proton-Coupled Electron Transfer in Organic Synthesis: Fundamentals, Applications, and Opportunities. *Top. Curr. Chem.* **2016**, *374*, 30. d) Gentry, E. C.; Knowles, R. R. Synthetic Applications of Proton-Coupled Electron Transfer. *Acc. Chem. Res.* **2016**, *49*, 1546–1556. e) Murray, P. R. D.; Cox, J. H.; Chiappini, N. D.; Roos, C. B.; McLoughlin, E. A.; Hejna, B. G.; Nguyen, S. T.; Ripberger, H. H.; Ganley, J. M.; Tsui, E.; Shin, N. Y.; Koronkiewicz, B.; Qiu, G.; Knowles, R. R. Photochemical and Electrochemical Applications of Proton-Coupled Electron Transfer in Organic Synthesis. *Chem. Rev.* **2022**, *122*, 2017–2291.